Analytical Methods

Accepted Manuscript

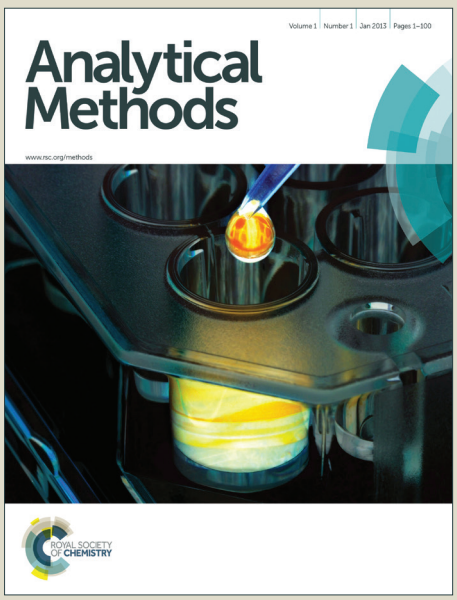

ROYAL SOCIETY OF CHEMISTRY

www.rsc.org/methods

An electrochemical sensor for honokiol based on a glassy carbon electrode modified with MoS_2/graphene nanohybrid film

Xiaojuan Zhao,[a,b] Xiaohong Xia,[a] Shengjiao Yu,[a] Chunming Wang*[a]

[a] School of Chemistry and Chemical Engineering, Lanzhou University, Lanzhou 730000, China

[b] Gansu College of Traditional Chinese Medicine, Lanzhou 730000, China

Abstract

A novel honokiol electrochemical sensor based on MoS_2/graphene nanohybrid was introduced in this work. The hybrid was characterized by X-ray diffraction, transmission electron microscopy, scanning electron microscopy and X-ray photoelectron spectroscopy. The electrochemical behavior of honokiol on the MoS_2/graphene modified glassy carbon electrode was investigated in pH 5.5 phosphate buffer solution by cyclic voltammetry and differential pulse voltammetry. Compared with bare glassy carbon electrode, the proposed electrode showed improved analytical performance characteristics in catalytic redox of honokiol. Under the optimal conditions, the modified electrode showed a linear voltammetric response to the honokiol with a concentration range from1.0×10^{-9} to 2.5×10^{-6} mol L^{-1}, and the detection limit (S/N=3) was estimulated at 6.2×10^{-10} mol L^{-1}. Moreover, the sensor also exhibited good reproducibility and stability, and could be used for the detection of honokiol in pharmaceutical samples.

Keywords: honokiol, graphene, MoS_2, electrochemistry, sensitive determination

1. Introduction

Honokiol (Fig. 1) is an effective component of the cortex of Magnolia Officinalis which is a useful Chinese herbal medicine prescribed in many formulas as an anodyne, a sedative, a stomach medicine or a cough remedy. Honokiol is reported to possess such functions as anti-inflammation [1], anti-tumor [2], anti-bacteria [3], arrhythmia-regulating [4], anti-platelet aggregation [5], and anti-oxidization [6]. The content of honokiol is an important parameter for evaluating the quality of Magnolia Officinalis. Therefore, it is greatly significant to develop some rapid, simple and sensitive

* Corresponding author at: School of Chemistry and Chemical Engineering, Lanzhou University, Lanzhou 730000, China. Tel.: +86 9318911895; fax: +86 9318912582. E-mail address: wangcm@lzu.edu.cn (C. Wang).

methods to determine the content of honokiol in Magnolia Officinalis. Until now, various methods such as high-performance liquid chromatography (HPLC) [7], capillary electrophoresis [8], liquid chromatography with mass spectrometry [9], synchronous fluorescence spectroscopy [10] and HPLC with electrochemical detection [11] are reported for the determination of honokiol. However, these techniques are time-consuming, expensive or require complicated pretreatment. Considering the inherent electrochemical activity of honokiol, an electrochemical scheme may be used in the determination of honokiol. In contrast to the above-mentioned methods, electroanalytical method exhibits many advantages such as high sensitivity, short analysis time, low cost and portability. In addition, electrochemical detection provides an opportunity to modify the electrode surface through the use of nano materials which can improve the analytical detection. For example, the carbon paste electrode (CPE) modified with nano-WO_3 was successfully employed to detect honokiol [12]. Besides, the glassy carbon electrode (GCE) coated with acetylene black nanoparticle was also applied for the electrochemical detection of honokiol [13]. However, to the best of our knowledge, there is no report based on graphene-modified electrode for the determination of honokiol.

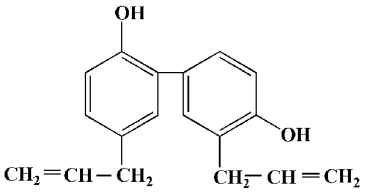

Fig. 1 Molecular structure of honokiol.

Graphene (GN), a monolayer of carbon atoms arranged in a two-dimensional honeycomb network, has attracted significant attention because of its large specific surface area and fascinating chemical, electronic and mechanical properties [14-16]. In addition, its easy processing, low cost in synthesis, and ability to form compounds with other materials make it an attractive candidate for fabricating various functional devices such as electrodes [17-20], sensors [21-23], photovoltaics [24] and photodetectors [25].

Since the discovery of the exotic properties of GN, the single-layer or few-layer transition metal disulfides have gained renewed interest [26, 27]. As a typical layered transition metal sulfide, MoS_2 has a structure analogous to that of GN, in which S-Mo-S layers are held together by van der Waals forces [28]. This layered structure has extremely low conductivity between adjacent S-Mo-S layers, which

leads to poor charge mobility. However, precisely because of this layered structure, atoms or molecules can be embedded by intercalation methods [29]. It is reported that the integration of carbon-based materials usually shows synergistic effects in electrocatalytic applications [30], so there is a reason to expect the integration of GN and layer-structured MoS_2 has the similar effect on the electrocatalysis and electrochemical sensors.

In the present work, an electrochemical sensor based on layered MoS_2/graphene (MoS_2/GN) hybrid film-modified glass carbon electrode (MoS_2/GN/GCE) was fabricated for the sensitive detection of honokiol in phosphate buffer solution (pH=5.5). The fabricated sensor showed excellent electrocatalytic activity on honokiol with a wider linear range and lower detection limit. In addition, the sensor also exhibited improved selectivity and acceptable reproducibility, and can be used for the detection of honokiol in real samples.

2. Experimental

2.1 Reagents and apparatus

Graphite powder (KS-10) and honokiol (＞99%) were purchased from Alfa Aesar (Beijing, China). Sodium molybdate ($Na_2MoO_4 \cdot H_2O$) and sulfocarbamide (NH_2CSNH_2) were obtained from Shanghai Reagent Co. (Shanghai, China). All other chemicals were of analytical reagent grades and used without further purification. Phosphate buffer solution (PBS, 0.2 M) was prepared by mixing the stock solution of 0.20 M NaH_2PO_4 and 0.2 M Na_2HPO_4, and the pH was adjusted by NaOH or H_3PO_4. All solutions were prepared with doubly distilled water, purified by Milli-Q system (Millipore Inc., nominal resistivity 18.2 MΩ cm).

All electrochemical experiments were performed on a CHI 660c electrochemical workstation (Shanghai Chenhua apparatus corporation, China). A standard three-electrode system was used with a saturated calomel electrode (SCE) as reference electrode, a platinum wire electrode as counter electrode and a bare or modified GCE as working electrode. The morphology of the samples was characterized by field-emission scanning electron microscopy (S-4800, Hitachi, Japan) and high-resolution transmission electron microscopy (HRTEM, Tecnai G2 F30, FEI, USA). The crystalline features of the samples were determined by X-ray powder diffraction (XRD, Rigaku D/max-2400). Chemical composition information about the samples was obtained by X-ray photoelectron

spectroscopy (XPS), the measurement was carried out on a multifunctional spectrometer (Thermon Scientific) using Al Kα radiation, and the binding energies were referenced to the C1s line at 284.8 eV from adventitious carbon. Inductively coupled plasma atomic emissions spetrometry (ICP-AES, IRIS Advantage) was applied to determine the content of MoS_2 in the nanohybrid.

2.2 Synthesis of MoS_2/GN

Graphene oxide (GO) was obtained from natural graphite powder by a modified Hummers method [31]. 30 mg GO was dissolved in 30 mL distilled water with ultrasonic treatment for 2 h to form a light yellow-brown suspension. Subsequently, 0.15 g $Na_2MoO_4 \cdot 2H_2O$ was added into the suspension. After ultrasonication and stirring for 20 min, 0.1 M NaOH was added to the solution until the pH value changed to 6.5. The overall volume was adjusted to 40 mL by adding doubly distilled water, in which 0.4 g sulfocarbamide (NH_2CSNH_2) was dissolved. Finally, the mixture solution was transferred into a Teflon-lined stainless steel autoclave (100 mL) and reacted at 220 °C for 24 h in an oven. The final product was separated by centrifuging and washed several times with distilled water and ethanol, respectively. Finally, the obtained hybrids were dried in a vacuum desiccator at room temperature. For comparison, GN and MoS_2 were achieved by the similar procedure.

2.3 Fabrication of electrochemical sensor

Prior to modification, the bare GCE was carefully polished to a mirror-like surface with 0.3, 0.05 μm alumina slurry, respectively. After successive sonication in ethanol and double distilled water, the electrode was rinsed with double distilled water and allowed to dry at room temperature. The MoS_2/GN was dissolved in dimethylformamide-nafion (49:1 volume ratio) at a concentration of 2.0 mg/mL with the aid of ultrasonic agitation for 30 min, resulting in a homogeneous black suspension. Afterward, 5 μL of MoS_2/GN solution was dropped on the pretreated GCE and dried at the room temperature, denoted as MoS_2/GN/GCE. For comparison, GN/GCE and MoS_2/GCE were also prepared by the same procedure. The fabrication process of the MoS_2/GN hybrid modified electrode is shown in Scheme 1.

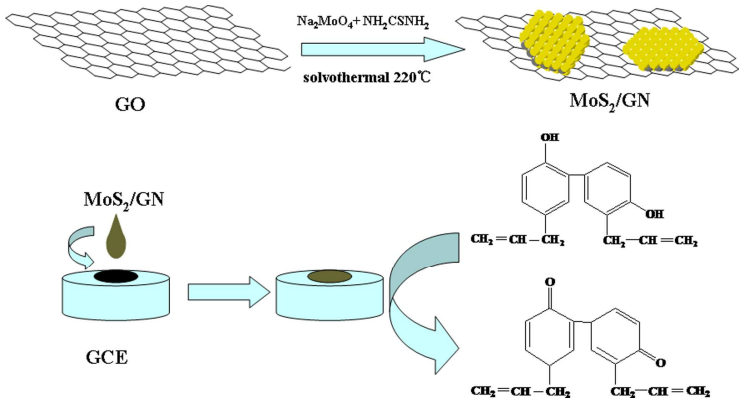

Scheme 1 Schematic diagram of the synthesis of MoS_2/GN hybrid and the fabrication process of the MoS_2/GN/GCE

2.4 Electrochemical measurements

The honokiol stocking solution was diluted to the required concentration by phosphate buffer solution (pH=5.5). The cyclic voltammetrys (CVs) were recorded in the potential range from 0.10 to 0.70 V at a scan rate of 100 mV s^{-1}. The differential pulse voltammetry (DPV) conditions were as follows: increment potential, 0.004 V; pulse amplitude, 0.05 V; pulse width, 0.05 s; sample width, 0.0167 s; pulse period, 0.2 s; and quiet time, 2 s.

2.5 Sample preparation

The Cortex Magnoliae Officinalis (i.e. Magnolia Bark) used in this study was purchased from a local Pharmacy. The Cortex Magnoliae Officinalis was dried at 60 °C for 2 h and was then pulverized. About 500 mg of powder was accurately weighed and dispersed in 20 mL ethanol. The mixture was kept in a 60 °C water bath for 3 h. After cooling, it was sonicated for 30 min and filtered through a filter paper. The above procedure was repeated with the bark residue. The extract was diluted exactly to 250 mL with ethanol, and this solution was used as the sample solution.

3. Results and discussion

3.1 Characterization of MoS_2/GN

Fig. 2 shows a general view of the morphologies of MoS_2 and MoS_2/GN that was synthesized by

hydrothermal method. As shown in Fig. 2A, the pristine MoS_2 obtained by the proposed method were prone to stack together. In strong contrast to the pristine MoS_2, when GO was predispersed in hydrothermal solution, the synthesized MoS_2/GN hybrid displayed a flower-like or three-dimensional architecture consisting of 2D nanoflakes (Fig. 2B). The 3D architecture of MoS_2/GN hybrid material was attributed to GN self-assembling during the hydrothermal process, in which GO was reduced to GN and the flexible GN self-assembles into a 3D architecture by partial overlapping or coalescing [32]. In the meanwhile, limited-layered MoS_2 with abundant exposed edge sites could grow restrictedly on the surface of GN sheets. The overlapping or coalescing of the GN can form an interconnected conducting network, and facilitate rapid electronic transport in electrode reactions. Furthermore, the 3D structure also enhances the stability of the MoS_2/GN composites due to superstrength of graphene. As an electrode material, this three-dimensional architecture with rough surface can enlarge the interfacial areas between the electrolyte/electrode and is advantageous in improving the sensitivity of the sensor. Fig. 2C, presenting the TEM image of MoS_2/GN, shows the MoS_2 sheets appeared in the form of loose and soft agglomerates of several nanometers. And Fig. 2D shows the MoS_2 sheets exhibited an interlayer distance of about 1.09 nm, which is in accordance with the result of XRD analysis.

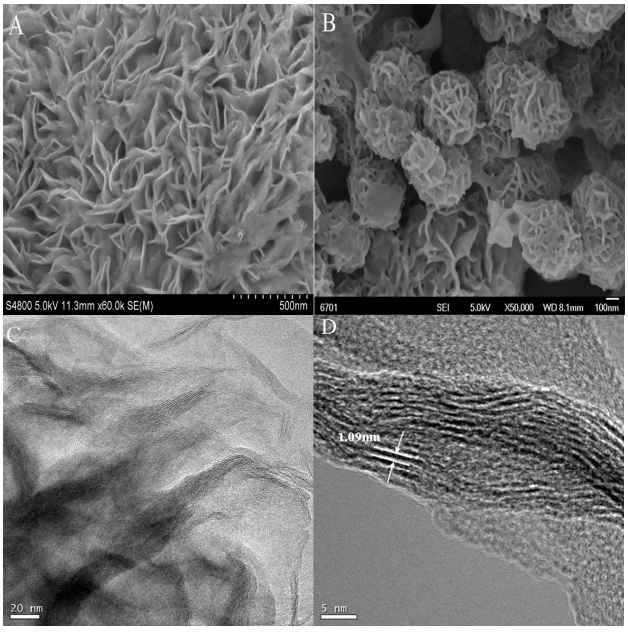

Fig. 2 (A) SEM image of MoS_2. (B) SEM image of MoS_2/GN. (C) TEM image of MoS_2/GN. (D) HRTEM of image of MoS_2 in MoS_2/GN hybrids.

The crystalline structures of GN, MoS_2, and MoS_2/GN nanohybrids have been characterized by XRD. In Fig. 3A (curve a), a broad diffraction peak (002) around 22.5° can be attributed to GN flake

[33]. In the pattern of MoS_2 (curve b), we can see that the major diffracted peaks are in agreement with the standard values in the standard card of MoS_2 (JCPDS 37-1492). For MoS_2/GN (curve c), a relatively strong and sharp diffraction peak at 2θ=8.1° could be attributed to the interlayer of the adjacent single-layer MoS_2 sheets. According to Bragg's equation, it can be calculated that the interlayer distance of the adjacent single-layer MoS_2 sheets in the hybrid is about 1.09 nm, which is much larger than that of standard MoS_2 (0.62 nm) [34]. It is probably because GN has inserted between two monolayers of MoS_2 and has enlarged the interlayer distance. Compared with the pattern of pristine MoS_2, the other feature peaks of MoS_2 have weakened. The reason for the change may be that the addition of GN has inhabited the growth of MoS_2 in some direction.

The components constituting MoS_2/GN nanohybrid has been further analyzed by XPS and it is found that it consisted of Mo, S, C, and O elements. It was calculated that the atomic ratio of Mo to S approaches the theoretical value of MoS_2 (1:2), confirming that the product was stoichiometric MoS_2. The oxygen element was from the GO, which were not reduced completely during hydrothermal reaction. The Mo 3d XPS spectra in Fig. 3B shows that the binding energies of Mo $3d_{5/2}$ and Mo $3d_{3/2}$ for MoS_2/GN occurred at 228.56 and 231.66 eV respectively, suggesting that Mo existed in the chemical state of Mo^{4+} [35]. At the same time, the S 2p spectra in Fig. 3C exhibited binding energies of S $2p_{3/2}$ and S $2p_{1/2}$ at 161.41 and 162.52 eV respectively. Further, the weight ratio of MoS_2 in the MoS_2/GN nanohybrid was obtained by using the inductively coupled plasma atomic emissions spetrometry. Through the calculation, we have found that the load of MoS_2 in the MoS_2/GN nanohybrid was 36.61%.

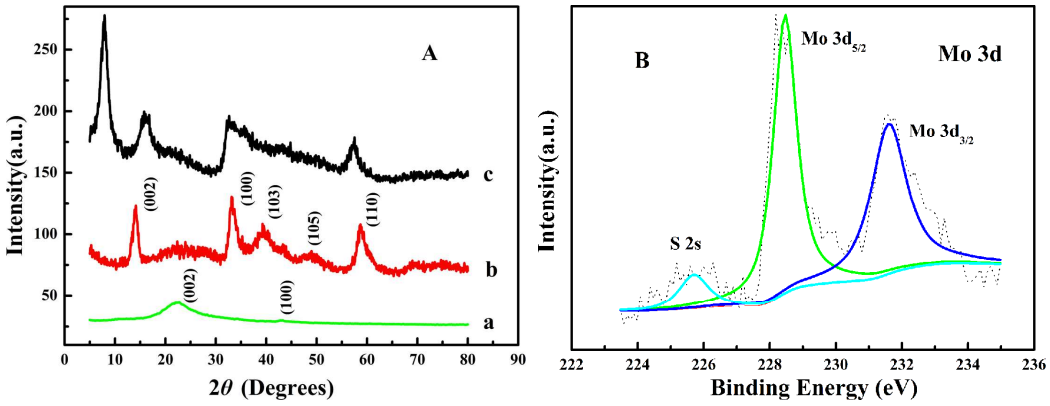

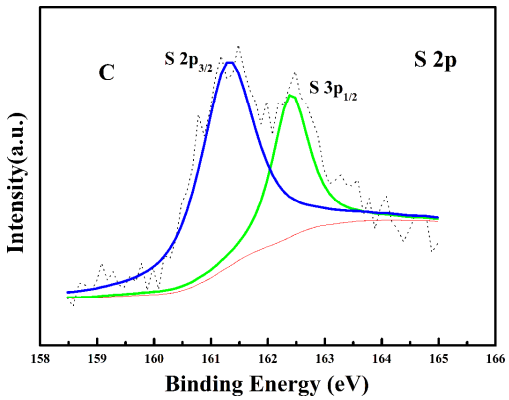

Fig. 3 (A) XRD patterns: (a) GN (b) MoS_2 and (c) MoS_2/GN. (B) Mo 3d and (C) S 2p XPS spectra of MoS_2 in MoS_2/GN hybrid.

3.2 Voltammetric behavior of honokiol

Fig. 4 exhibits the CV responses of 5 μM honokiol in 0.2 M PBS (pH=5.5) on different electrodes. In a blank buffer solution (inset of Fig. 4), no redox peak was observed on MoS_2/GN/GCE, indicating that the MoS_2/GN/GCE was non-electroactive in the selected potential region. For the bare GCE (curve a), honokiol gave a rather small CV peak. When the GCE was modified with a layer of MoS_2, the redox peak currents increased slightly (curve b). Similarly, when the GCE was modified by GN (curve c), the redox peak currents increased up to 10 times that on the bare GCE, which might be attributed to the excellent conductivity and large surface area of GN. Therefore, compared with other electrodes, the MoS_2/GN/GCE (curve d) showed the largest redox peak currents, about 25 times higher than those on the bare GCE. Moreover, a pair of well-defined and quasi-reversible redox peaks of honokiol were obtained at E_{pa}=0.436 V and E_{pc}=0.365 V. It is an obvious fact that the response of the honokiol on the electrode is significantly enhanced after being modified by MoS_2/GN. This may be related to the more efficient interface and microenvironment provided by the surface of the MoS_2/GN for the electrochemical reactivity of honokiol.

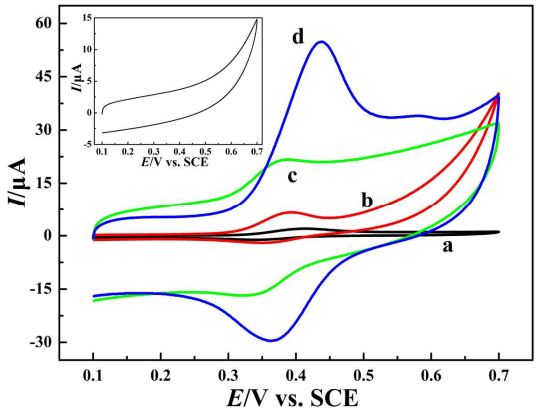

Fig. 4 Cyclic voltammograms on the (a) bare GCE, (b) MoS_2/GCE, (c) GN/GCE, (d) MoS_2/GN/GCE in 0.2 M PBS (pH=5.5) containing 5 μM honokiol at scan rate of 100 mV s^{-1}. Inset: the cyclic voltammogram of MoS_2/GN/GCE in 0.2 M PBS (pH=5.5) without honokiol.

3.3 Effect of scan rate

To investigate the reaction kinetics of honokiol on the MoS_2/GN/GCE, the responses of honokiol at various scan rates from 25 to 350 mV s^{-1} were tested by CV. From Fig. 5A, the peak currents of honokiol increased with scan rate. Moreover, the oxidation (I_{pa}) and reduction (I_{pc}) peak currents for honokiol increased linearly with the square root scan rate in the range of 25-350 mV s^{-1} (Fig. 5B) and the linear relationship could be expressed by I_{pa} (μA) = $9.31v^{1/2}$ (mV $s^{-1})^{1/2}$-30.35 and I_{pc} (μA) = $-5.97v^{1/2}$ (mV $s^{-1})^{1/2}$+26.33 with the R=0.9911 and 0.9969 respectively. The results indicate that the electrochemical reaction of honokiol on modified electrode is a diffusion-controlled process.

Moreover, with the increase in scan rate, the oxidation peak potential shifted positively while the reduction peak potential shifted negatively. At higher scan rates, the anode (E_{pa}) and cathode (E_{pc}) peak potentials had a linear relationship with the logarithm of scan rates (log v). When scan rates range from 150 to 350 mV s^{-1} (Fig. 5C), the linear regression equations of the E_{pa} and E_{pc} *vs.* log v are expressed as E_{pa} (V)=0.5661+0.08588log$v$ (V s^{-1}) and E_{pc} (V)=0.2904-0.07181log$v$ (V s^{-1}) with R=0.9975 and 0.9978 respectively. According to Laviron's model [36], the slope of the line for E_{pa} and E_{pc} can be expressed as $2.303RT/(1-\alpha)nF$ and $-2.303RT/\alpha nF$ respectively. Therefore, the value of the electron-transfer coefficient (α) and the electron-transfer number (n) were calculated as 0.54 and 2 respectively.

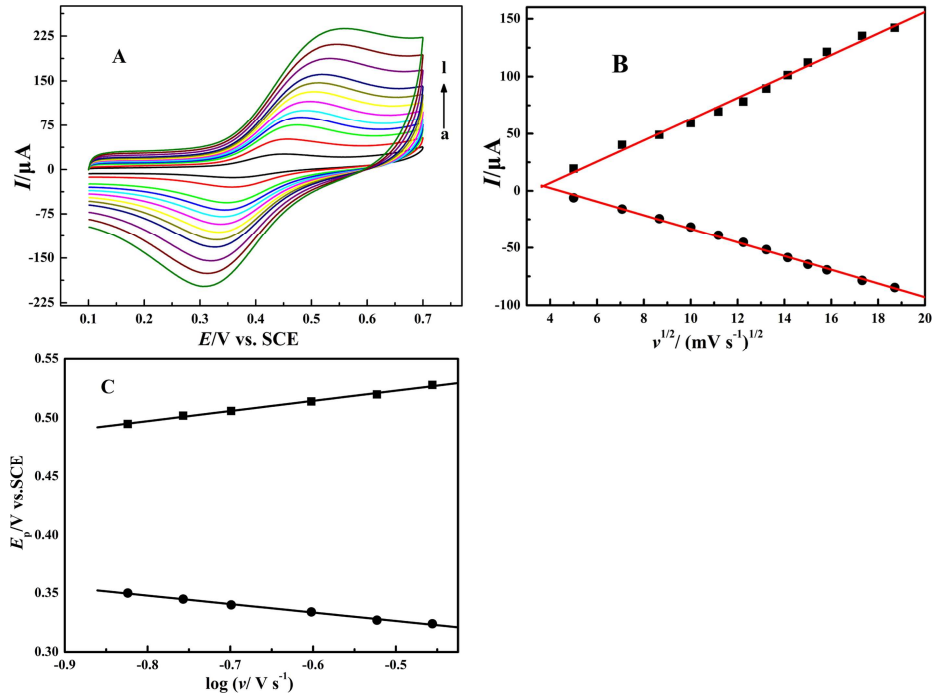

Fig. 5 (A) Cyclic voltammograms of 5 μM honokiol on the MoS_2/GN/GCE at different scan rates (25, 50, 75, 100, 125, 150, 175, 200, 225, 250, 300, 350 mV s^{-1}) in 0.2 M PBS (pH=5.5). (B) The plot of the redox peak current versus the square root of scan rate. (C) Plots of anodic and cathodic potentials against the logarithmic of scan rate.

3.4 Effect of accumulation time

The accumulation time is another key factor for electroanalysis. Here, we investigated the effect of the accumulation time in 5 μM honokiol solution on MoS_2/GN/GCE. As shown in Fig. 6A, the oxidation peak current of honokiol increased greatly with the accumulation time and reached a maximum after 200 s and then stabilizes, indicating that 200 s is sufficient to reach the honokiol saturation on MoS_2/GN/GCE. Therefore, 200 s was selected as the accumulation time.

3.5 Effect of pH

The pH of the supporting electrolyte shows a significant effect on the electrochemical behavior of honokiol on MoS_2/GN/GCE. The CV was carried out to characterize the influence of pH of the buffer solution (in the range of 4.5-7.0) on it. According to Fig. 6B, a maximum current was obtained at pH 5.5. Therefore, pH 5.5 was selected as the optimum pH. Furthermore, it can be seen that when the pH

of the medium gradually increased, the potential shifted towards less positive values. Over the pH range of 4.5-7.0, the redox potential changed linearly with pH value. The relationships between potential and pH are expressed by the following equations: E_{pa} (V) =0.7436-0.05526pH (R=0.9957) and E_{pc} (V) =0.6940-0.06023pH (R=0.9990). According to the following formula [36]: $dE_p/dpH=2.303mRT/nF$ (*m* is the number of protons and *n* is the number of electrons), *m*/*n* was calculated to be 0.93 and 1.02 for the oxidation and reduction processes respectively. These reveal that an equal number of protons and electrons were involved in the reduction reactions of honokiol. And the electrode reaction equation can been expressed as Fig. 7.

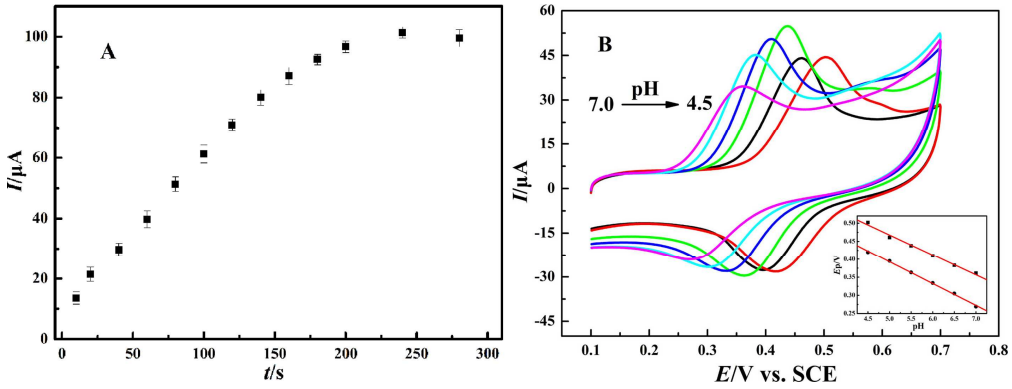

Fig. 6 (A) The effect of accumulation time on the peak current of honokiol. (B) Cyclic voltammograms of 5 μM honokiol on the MoS_2/GN/GCE in 0.2 M PBS in different pH values (4.5, 5.0, 5.5, 6.0, 6.5, 7.0) at scan rate of 100 mV s^{-1}. Inset: the plot of anodic and cathodic peak potentials of honokiol versus pH values

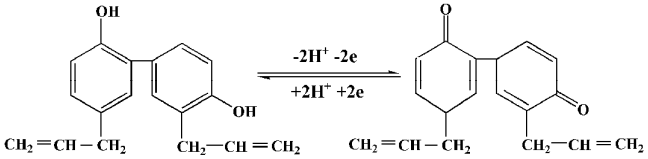

Fig. 7 The electrode-reaction equation of honokiol

3.6 Determination of honokiol

Under the optimal conditions, DPV was employed for the quantitative analysis of honokiol over the concentration range of 0.001-2.5 μM. Fig. 8A shows the DPVs for different concentrations of honokiol on the MoS_2/GN/GCE in pH 5.5 PBS. Obviously, there was an enhancement in its oxidation peak current with the increase of the honokiol concentration, suggesting that the MoS_2/GN/GCE can be applied to the quantitative determination of honokiol. Fig. 8B shows the logarithm of oxidation peak

current had a good linear relationship with the logarithm of honokiol concentration in the range from 1.0×10^{-9} to 2.5×10^{-6} mol L^{-1}. The regression equation is log I_{pa} (μA)=1.6512+0.6879log$C$ (μM) with R=0.9952. The detection limit (S/N=3) was estimated to be about 6.2×10^{-10} mol L^{-1}. The results show that the performances of the MoS_2/GN/GCE are comparable or superior to some reported methods (Table 1). Therefore, the MoS_2/GN/GCE sensor can serve as a good platform for the determination of honokiol.

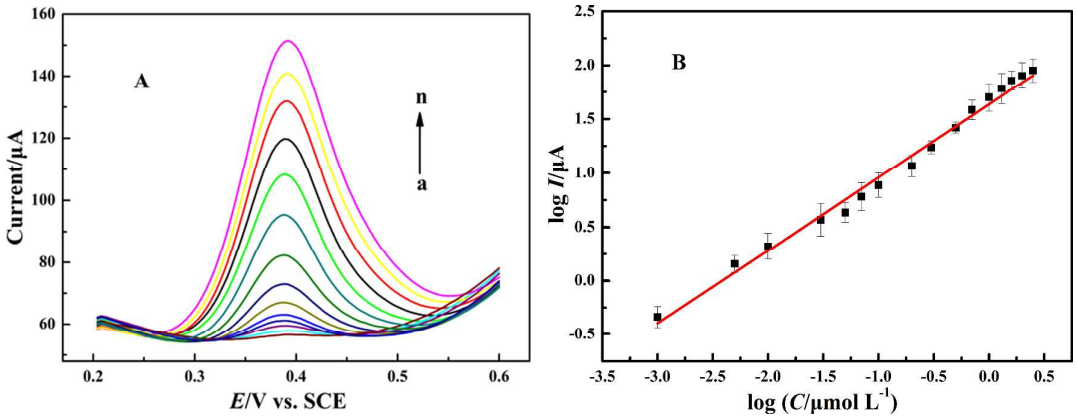

Fig. 8 (A) Differential pulse voltammograms of 0.001, 0.005, 0.01, 0.03, 0.07, 0.1, 0.2, 0.3, 0.5, 0.7, 1.0, 1.3, 1.6, 2.0 and 2.5 μM honokiol on MoS_2/GN/GCE in 0.2 M PBS (pH 5.5). (B) Concentration calibration curve of the differential pulse voltammetry current response for honokiol.

Table 1 Comparison of proposed method for determination of honokiol with others.

Method	Linear range/μmol L^{-1}	LOD/μmol L^{-1}	Ref.
HPLC	0.075–0.75	–	[7]
LC-MS/MS	0.0094–1.88	–	[9]
Flow injection-capillary electrophoresis	18.8–1126	2.4	[38]
Nano-WO_3/CPE[a]	0.03–20	0.01	[12]
CNT/PMMA[b] composite disc electrode	0.0019–1.126	0.0094	[13]
Mesoporous SiO_2/CPE	0.0075-0.375	0.0018	[37]
Acetylene black film-modified electrode	0.05-20	0.008	[39]
RGO[c]-WO_3 nanowire modified GCE	0.01-20	0.008	[40]
MoS_2/GN/GCE	0.001-2.5	0.00062	This work

[a] Carbon paste electrode.

[b] Poly(methyl methacrylate).

[c] Reduced Graphene Oxide

3.7 Reproducibility of MoS_2/GN/GCE and Interference studies

The reproducibility of the sensor was tested by detecting the DPV response of 1 μmol L^{-1} honokiol in 0.2 M PBS (pH = 5.5) with the same electrode ten times. The result shows that the RSD of the detection was 4.38%, indicating that the MoS_2/GN/GCE had good reproducibility. The long-term stability of the sensor was evaluated by measuring its performance after being stored at 4 °C for a period of time. The sensor retained about 94% of initial response after a week, which suggests acceptable stability.

To assess the selectivity of the MoS_2/GN/GCE for honokiol, various potential interfering species were examined in connection with their effects on the determination of honokiol. Some species commonly existing in biological samples were chosen for a fixed honokiol concentration of 1.0×10^{-6} mol L^{-1}. The inorganic species K^+, Na^+, Ca^{2+}, Mg^{2+}, Zn^{2+}, Cu^{2+}, Al^{3+}, Cl^-, NO_3^-, and SO_4^{2-} in a 100-fold concentrations almost have no influence on the detection of honokiol since the peak current change is below 5%. Moreover, 50-fold concentrations magnolol, hydroquinol, quercitrin and 100-fold concentrations of ascorbic acid, dopamine, catechol, and glucose didn't show interference, too.

3.8 Detection of honokiol in real samples

The determination of honokiol in cortex Magnoliae Officinalis was applied to the evaluation of the applicability of the modified electrode. The tests were conducted in triplicate by the standard addition method, and the results obtained are shown in Table 2. The recovery of three independent experiments varied from 99.20% to 101.23%. These results indicate that the MoS_2/GN/GCE is suitable for the determination of honokiol in real samples.

Table 2 Determination of honokiol in pharmaceutical samples.

Sample	Measured[a] /μmol L^{-1}	Add/μmol L^{-1}	Found/μmol L^{-1}	RSD (%)	Recovery (%)
1	0.96	0.5	1.48±0.07	2.97	101.02
2	0.97	1.0	1.95±0.16	5.17	99.20
3	0.94	1.5	2.47±0.13	3.85	101.23

[a] 50 μL of the sample solution (section 2.5) was added into an electrochemical cell and the volume was made up to

5 mL with 0.2 M PBS(pH =5.5).

4. Conclusions

In this work, a novel honokiol electrochemical sensor based on MoS_2/GN hybrid was introduced. The sensor exhibited an excellent electrochemical activity for honokiol. Under the optimal conditions, the MoS_2/GN/GCE displays wider linear range, lower detection limit, superior selectivity and higher stability in honokiol detection. In addition, the sensor also has good recoveries and can be applied to determinate honokiol in real samples. From the above results, we can conclude that the MoS_2/GN hybrid can be used as a promising electrode material in pharmaceutical analysis.

Acknowledgment

This work is financially supported by the National Nature Science Foundation of China (NO.51372106).

References

1 J. Park, J. Lee, E. S. Jung and Y. Park, *Eur. J. Pharm.*, 2004, **496**, 189–195.

2 K. Ikeda, Y. Sakai and H. Nagase, *Phytother. Res.,* 2003, **7**, 933–937.

3 K. Y. Ho, C. C. Tsai, C. P. Chen, J. S. Huang and C. C. Lin, *Phytother. Res.*, 2001, **15**, 139–141.

4 S. K. Tsai, C. H. Huang, S. S. Huang, L. M. Hung and C. Y. Hong, *Pharmacology*, 1999, **59**, 227–233.

5 M. K. Pyo, Y. Lee and H. S. Yun-Choi, *Arch. Pharm. Res.*, 2002, **25**, 325–328.

6 M. Ogata, M. Hoshi, K. Shimotohno and S. Urano, *J. Am. Oil Chem. Soc.*, 1997, **74**, 557–562.

7 X. N. Wu, X. G. Chen and Z. D. Hu, *Talanta*, 2003, **59**, 115–121.

8 Z. P. Zhang, Z. D. Hu and G. L. Yang, *Microchim. Acta*, 1997, **127**, 253–258.

9 Y. T. Wu, L. C. Lin and T. H. Tsai, *Biomed. Chromatogr.*, 2006, **20**, 1076–1081.

10 M. Zhang and L. M. Du, *Chin. Chem. Lett.*, 2006, **17**, 1603–1606.

11 A. Kotani, S. Koilma, H. Hakwata, D. Jin and F. Kusu, *Chem. Pharm. Bull.*, 2005, **53**, 319–322.

12 W. Y. Qu, X. Y. Xiong, W. B. Hu, P. Zhang, Q. Luo and S. H. Zhang, *Colloids and Surfaces B: Biointerfaces*, 2012, **100**, 103–106.

13 X. F. Yang, M. M. Gao, H. D. Hu and H. J. Zhang, *Phytochem. Anal.*, 2011, **22**, 291–295.

14 H. L. Wang, L. F. Cui, Y. Yang, H. S. Casalongue, J. T. Robinson, Y. Y. Liang, Y. Cui and H. J. Dai, *J. Am. Chem. Soc.*, 2010, **132**, 13978–13980.

15 Z. S. Wu, D. W. Wang, W. C. Ren, J. P. Zhao, G. M. Zhou, F. Li and H. M. Cheng, *Adv. Funct. Mater.*, 2010, **20**, 3595–3602.

16 H. L. Wang, H. S. Casalongue, Y. Y. Liang and H. J. Dai, *J. Am. Chem. Soc.*, 2010, **132,** 7472–7477.

17 M. Zhou, Y. M. Zhai and S. J. Dong, *Anal. Chem.* 2009, **81**, 5603–5613.

18 C. X. Guo, Y. Lei., C. M. Li, *Electroanal.* 2011, **23**, 885-893.

19 K. J. Huang, Y. J. Liu, J. T. Cao, H. B. Wang, *RSC Adv.*, 2014, **4**, 36742-36748.

20 K. J. Huang, Y. J. Liu, H. B. Wang, T. Gan, Y. M. Liu, L. L. Wang, *Sensor. Actuat. B-Chem.*, 2014, **191**, 828-836.

21 G. P. Kotchey, B. L. Allen, H. Vedala, N. Yanamala, A. A. Kapralov, Y. Y. Tyurina, J. Klein-Seetharaman, V. E. Kagan and A. Star, *ACS Nano*, 2011, **5**, 2098–2108.

22 C. X. Guo, Z. S. Lu, Y. Lei, C. M. Li, *Electrochem. Commun.*, 2010, **12**, 1237-1240.

23 C. X. Guo, S. R. Ng, S. Y. Khoo, X. T. Zheng, P. Chen, C. M. Li, *ACS Nano*, 2012, **6**, 6944-6951.

24 Z. Y. Yin, S. Y. Sun, T. Salim, S. X. Wu, X. A. Huang, Q. Y. He, Y. M. Lam and H. Zhang, *ACS Nano*, 2010, **4**, 5263–5268.

25 S. Ghosh, B. K. Sarker, A. Chunder, L. Zhai and S. I. Khondaker, *Applied Physics Letters*, 2010, 96, 163109.

26 C. N. R. Rao and A. Nag, *Eur. J. Inorg. Chem.*, 2010, **27**, 4244–4250.

27 K. J. Huang, L. Wang, Y. J. Liu, T. Gan, Y. M. Liu, L. L. Wang, Y. Fan, *Electrochim. Acta*, 2013,**107**, 379-387

28 Q. S. Gao , C. Giordano and M. Antonietti , *Angew. Chem. Int. Ed.*, 2012, **51**, 11740–11744.

29 Z.Y. Wang, H. Li, Z. Liu, Z. J. Shi, J. Lu, K. Suenaga, S. K. Joung, T. Okazaki, Z. N. Gu and J. Zhou, *J. Am. Chem. Soc.*, 2010, **132**, 13840-13847.

30 Y. L. Yao, Y. Ding, L. S. Ye and X. H. Xia, *Carbon*, 2006, **44**, 61–66.

31 W. S. Hummers and R. E. Offeman, *J. Am. Chem. Soc.*, 1958, **80**, 1339-1339.

32 Y. X. Xu, K. X. Sheng, C. Li and G. Q. Shi, *ACS Nano*, 2010, **4**, 4324–4330.

33 K. P. Liu, J. J. Zhang, G. H. Yang, C. M. Wang and J. J. Zhu, *Electrochem. Commun.*, 2010, **12**,

402–405.

34 K. Chang and W. X. Chen, *J. Mater. Chem.*, 2011, **21**, 17175–17184.

35 W. K. Ho, J. C. Yu, J. Lin, J. G. Yu and P. S. Li, *Langmuir*, 2004, **20**, 5865–5869.

36 E. Laviron, *J. Electroanal. Chem.*, 1979, **101**, 19–28.

37 J. Zhao, W. S. Huang and X. J. Zheng, *J. Appl. Electrochem.*, 2009, **39**, 2415–2419.

38 L. H. Liu, X. Wu, L. Y. Fan, X. G. Chen and Z. D. Hu, *Anal. Bioanal. Chem*., 2006, **384**, 1533-1539.

39 W. S. Huang, X. J. Zheng, D. Z. Zhu, K. B. Wu, *Electrochem. Solid-State Lett.*, 2008, **11**, F16-F18.

40 M. Huang, Y. Wu, W. B. Hu, *Ceram. Int.*, 2014, **40**, 7219-7225.

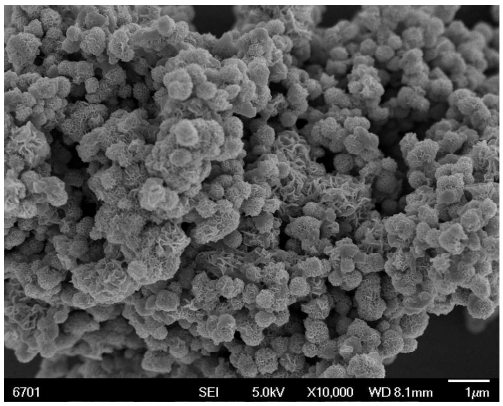

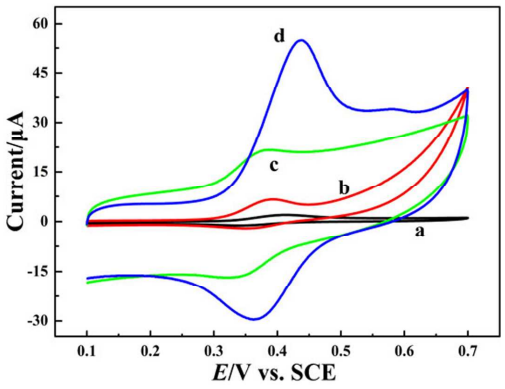

An electrochemical sensor for sensitive determination of honokiol was successfully constructed based on MoS_2/graphene nanohybrid.